Supporting Information

Interfacial Electronic Engineering of Co-doped $Ni(OH)_2$ Nanoarrays for Efficient Electrooxidation of Xylose to Formate

Jianyun Gan[a], Ning Wang[a], Yunpeng Liu[b], Zhendong Liu[a], Bo Lu[a], Yongfa Huang[a], Ge Yuan[a], Emmanuel Iwuoha[c], Ruidong Xia[d], Ren Zou[a,*], Xinwen Peng[a,*]

[a] *School of Light Industry and Engineering, South China University of Technology, Guangzhou 510641, China*

[b] *School of Materials Science and Energy, Foshan University, Foshan, 528231, China*

[c] *Sensor Lab (UWC Sensor Laboratories), Department of·Chemistry, University of the Western Cape, Bellville, Cape·Town·7535, South·Africa*

[d] *State Key Laboratory of Organic Electronics and Information Displays & Institute of Advanced Materials (IAM), School of Materials Science and Engineering, Nanjing University of Posts and Telecommunications, Nanjing 210023, China*

*****Corresponding author: School of Light Industry and Engineering, South China University of Technology, Guangzhou 510641, China*

***E-mail**: fexwpeng@scut.edu.cn (X. Peng)*

1. Experimental Section

1.1. Chemicals: Nickel(II) nitrate hexahydrate ($Ni(NO_3)_2·6H_2O$), Cobalt(II) nitrate hexahydrate ($Co(NO_3)_2·6H_2O$), urea (CH_4N_2O), NH_4F, ethanol (CH_3CH_2OH), Formic Acid (HCOOH), xylose ($C_5H_{10}O_5$) and potassium hydroxide (KOH) were purchased from Aladdin Industrial Corporation.

1.2. Pre-treatment of carbon felt (CF).

The CF was cut into slices (~3 cm × 4 cm, 2 mm in thickness) which was washed alternately with ethanol and deionized water three times and dried under vacuum at 60 ℃ overnight.

1.3. Preparation of Co-doped $Ni(OH)_2$@CF

1.8 mmol of $Ni(NO_3)_2·6H_2O$, 0.2 mmol $Co(NO_3)_2·6H_2O$, 8 mmol of NH_4F and 0.8 g of urea were added into 30 mL of ultrapure water with stirring. A piece of cleaned carbon felt (2 cm × 3 cm, 2 mm in thickness) was placed in a 50 mL Teflon-lined autoclave. Then, the well-mixed solution was transferred into the above vessel and heated at 120 °C for 6 h. After washed with deionized water and ethanol for several times, the Co-$Ni(OH)_2$ was obtained (~30 mg cm^{-2}). During the hydrothermal process, a series of Co doping ratios (0, 0.1, 0.2, 0.3, 0.4 mmol) were adopted to optimize electrocatalytic performance.

1.4. Materials Characterization

The morphology and microstructure of the electrocatalyst were characterized by scanning electron microscopy (SEM, SU8600), scanning transmission electron microscopy (TEM, 2100), Raman spectrometer (LabRamHR) with a 532 nm excitation laser. Powder X-ray diffraction (XRD, Bruker D8) was conducted using an X-ray diffractometer with graphite monochromatized Cu Kα irradiation (λ=1.54 Å).

X-ray photoelectron spectroscopy (XPS) data were measured with an X-ray photoelectron spectrometer (Thermo Scientific K-Alpha). The inductively coupled plasma optical emission spectroscopy (ICP–OES, Agilent 720) was conducted to determine the actual weight loading of Co and Ni. X-ray absorption fine structure (XAFS) spectra of Co K-edge were recorded in transmission mode on Table XAFS-500A (Specreation Instruments Co., Ltd.) at 25 kV and 20 mA. The Si (533) spherically

bent crystal analyzer with a radius of curvature of 500 mm was used.

2. Electrochemical measurements.

The electrocatalytic tests were conducted using an electrochemical workstation (CHI760E). The Co-Ni$(OH)_2$@CF (~0.5 cm × 0.5 cm) were directly used as work electrode, a Pt foil was used as the counter electrode, and a standard Ag/AgCl electrode was used as the reference electrode. The OER were tested in 1.0 M KOH electrolyte solution. The electrocatalytic oxidation of xylose were tested in 40 ml 1.0 M KOH with 100 mM xylose. The potentials were converted to the reversible hydrogen electrode (RHE) through the Nernst equation: ($E_{(RHE)}=E_{(Ag/AgCl)}+0.0591$ pH + 0.197 $V_{).}$ The scan rate for LSV was kept at 2 mV s^{-1}. *IR* compensation was employed in each electrochemical measurement. The correction potential (E_{corr}) was obtained by equation:

$$E_{corr} = E_{mea} - iR_s$$

where E_{mea} and R_s are measured potential and solution resistance, respectively.

The Tafel plots was assessed by equation:

$$n = b\log j + a$$

where b and j are Tafel slope and current density, respectively.

The electrochemical surface area (ESCA) was evaluated in terms of the double-layer capacitance (C_{dl}). Cyclic voltammetry (CV) was performed in 1.0 M KOH at different scan rates of 20, 40, 60, 80, 100, 120 mV s^{-1} in a potential window where no Faradaic process occurs.

Operando electrochemical impedance spectroscopy (EIS) measurements were conducted with a three-electrode system. The frequency ranged from 100000 to 0.01 Hz with an amplitude of 5 mV s^{-1}.

The XOR experiments were carried out in a three-electrode system by constant voltage from 1.50 V_{RHE} to 1.70 V_{RHE}. The electrocatalyst solution consists of 8 mL 1.0 M KOH with 0.1 M xylose, which the electrolytes product of XOR was analyzed using high-performance liquid chromatography (LC5090Plus, Fuli Instruments) with an ultraviolet-visible detector set at 210 nm, 5 mM H_2SO_4 was used as the mobile phase at

35 °C with a flow rate of 0.6 mL min^{-1}. The scaled up XOR experiments were carried out in a flow cell electrochemical reactor (WuhanZhisheng New Energy Co., Ltd.). The $Co_{0.2}$-$Ni(OH)_2$@CF (2 cm × 2 cm, 2 mm in thickness) were directly used as work electrode. An anion exchange membrane (FAA-3-PK-130) was used to separate the anode and cathode compartments. The electrolyte consisted of 450 mL of 1.0 M KOH containing 0.1 M xylose. A peristaltic pump circulated the electrolyte through the reactor at a constant flow rate of 20 mL min^{-1}. In addition, the electrolysis reaction was performed at room temperature with a constant current of 1 A. The product was confirmed by HPLC spectroscopy.

$$\text{Yield of Formate (\%)} = \frac{Moles\ of\ product \times carbaon\ numbers\ in\ product}{Moles\ of\ product \times carbaon\ numbers\ in\ substrate} \times 100\%$$

The Faradaic efficiency (FE) of Formate production was calculated using equations:

$$\text{FE (\%)} = \frac{\text{mol of FA}}{\text{total charge passed}/(2 \times \text{F})} \times 100\%$$

Here, F is the Faraday constant (96485 C mol^{-1}).

Formate production rate (mmol h^{-1}) was calculated as shown in:

$$\text{Formate production rate} = \frac{\text{m} \times \text{volume}}{\text{t}} \times 100\%$$

Where m is the concentration of main products (mol L^{-1}), and t is the reaction time (h).

The electricity consumption per m^3 of H_2 produced was calculated as follows:

$$W = \frac{n \times F \times U \times 1000}{3600 \times V_m}$$

Where n is the molarity of electrons transferred for product, U is the input voltage and V_m is the molar volume of the gas at standard atmospheric pressure (22.4 mol L^{-1}). It is noted that $n = 2$ for biomass electrooxidation-coupled a cathode-only hydrogen production system.

Supplement Results

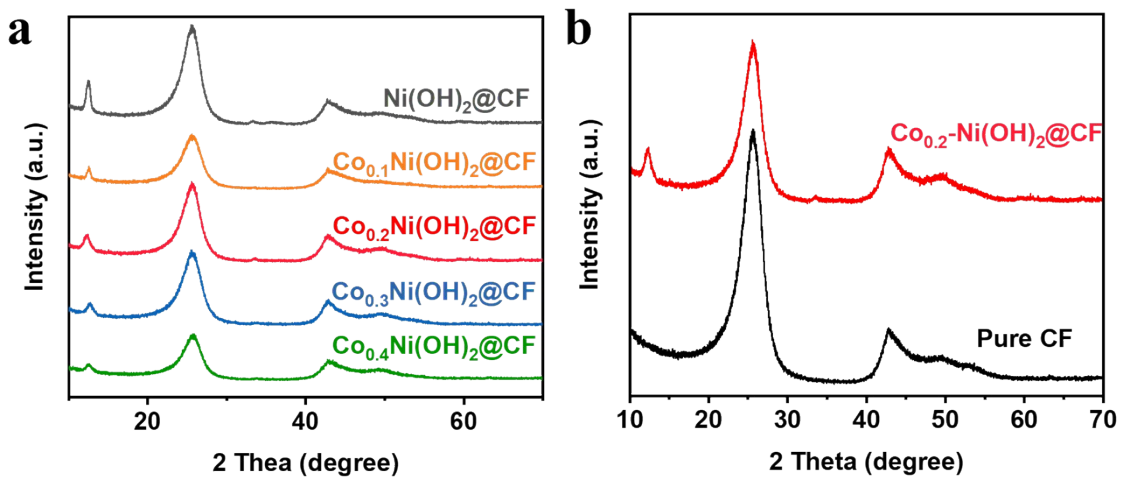

Fig. S1 XRD spectrum of (a) $Co_xNi(OH)_2$@CF and (b) CF.

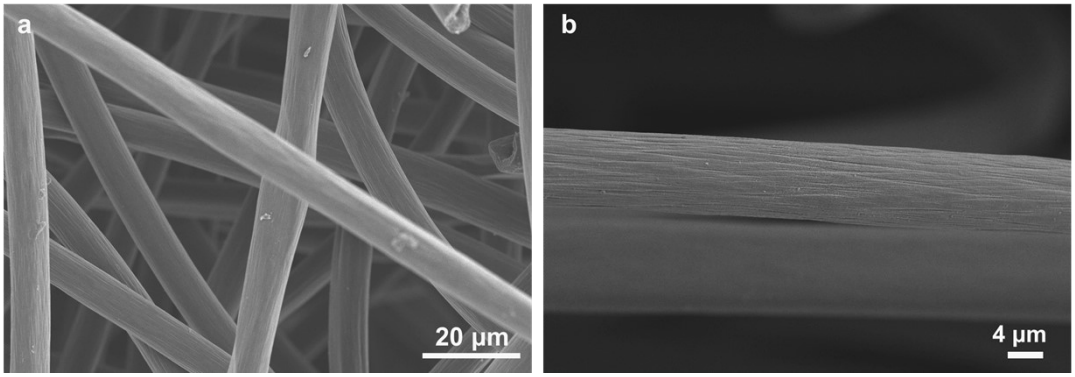

Fig. S2 (a, b) SEM images of pure Carbon Felt (CF).

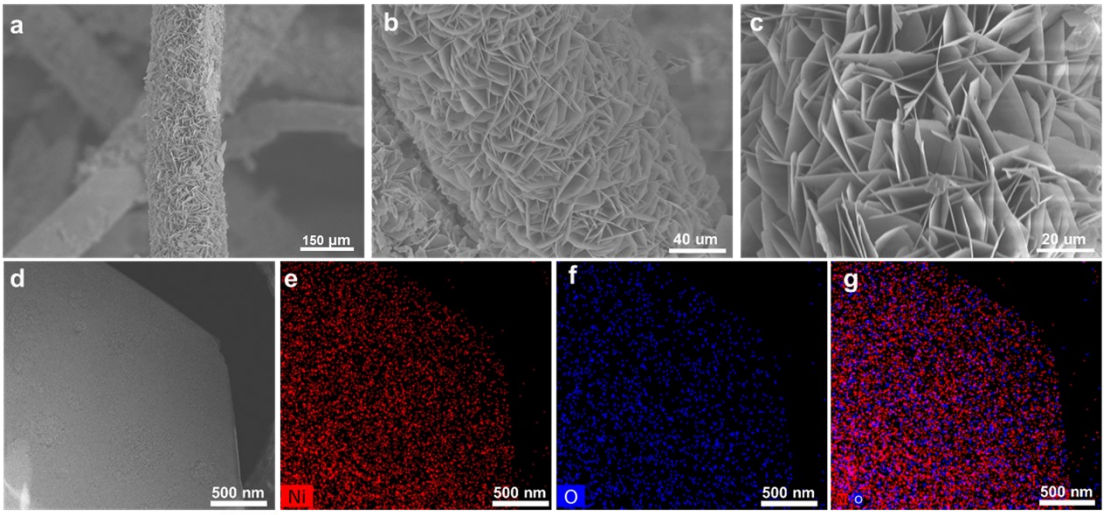

Fig. S3 The $Ni(OH)_2$@CF of SEM (a-d) image and (e-g) mapping.

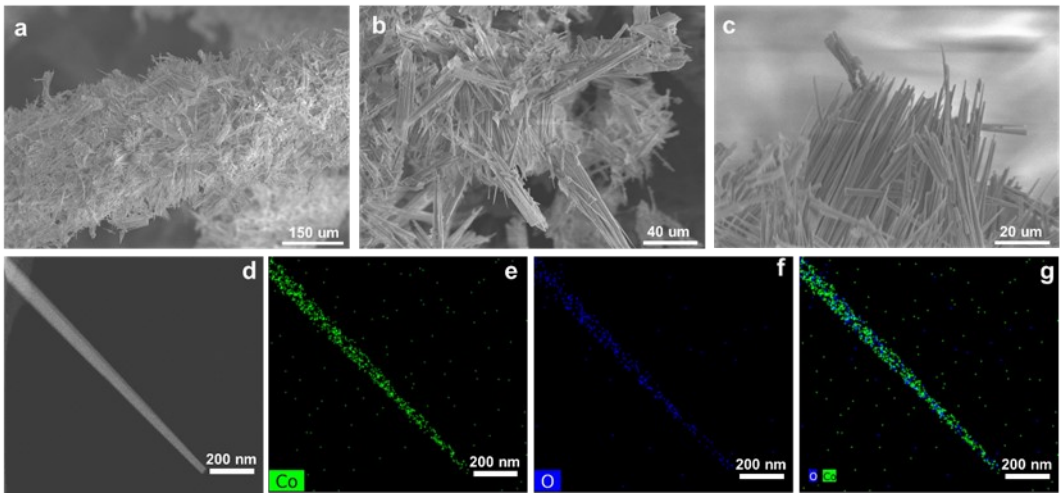

Z

Fig. S4 The $Co(OH)_2$@CF of SEM (a-c) image, TEM (d) image and (e-g) mapping.

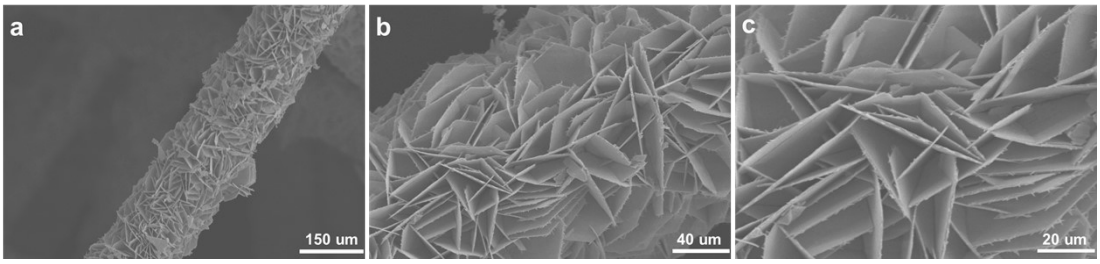

Fig.S5 The $Co_{0.2}$-$Ni(OH)_2$@CF of SEM image.

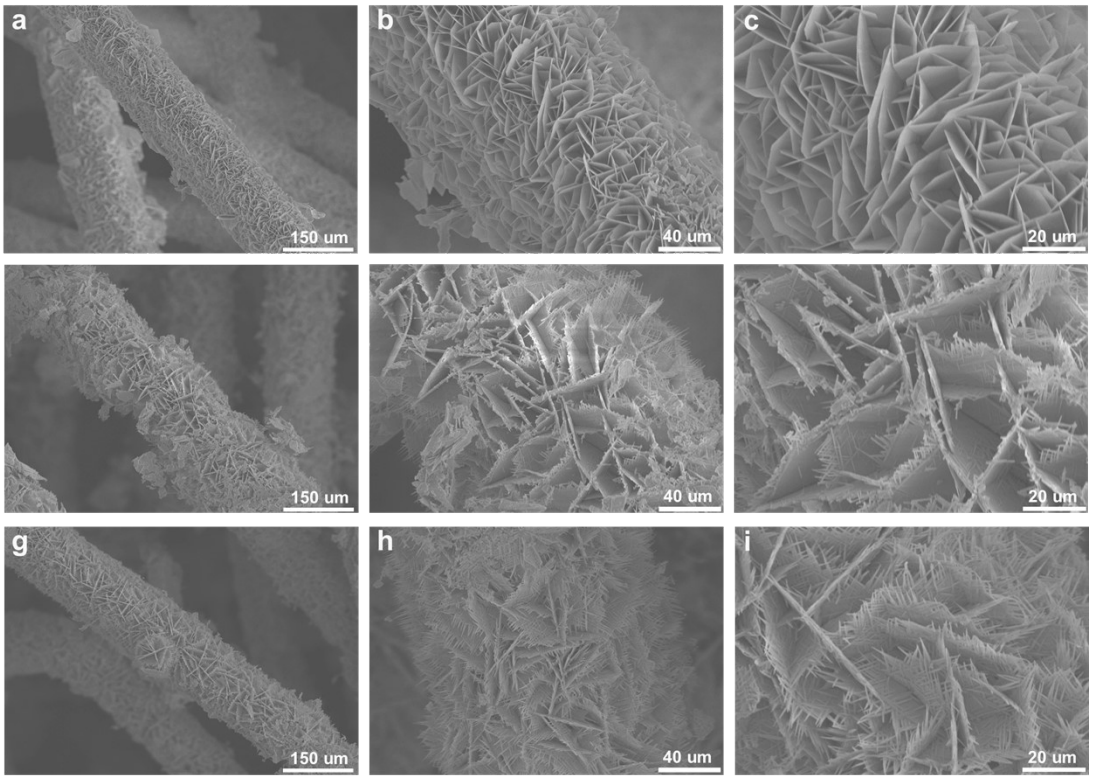

Fig. S6 The SEM image of $Co_{0.1}$-$Ni(OH)_2$@CF (a-c), $Co_{0.3}$-$Ni(OH)_2$@CF (d-f), and $Co_{0.4}$-$Ni(OH)_2$@CF (g-i).

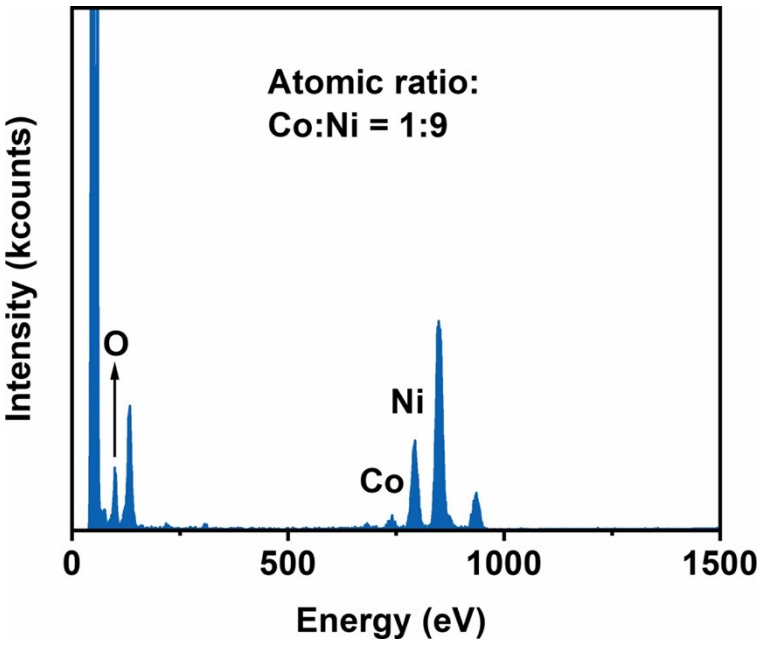

Fig. S7 EDX spectrum of the $Co_{0.2}$-$Ni(OH)_2$@CF.

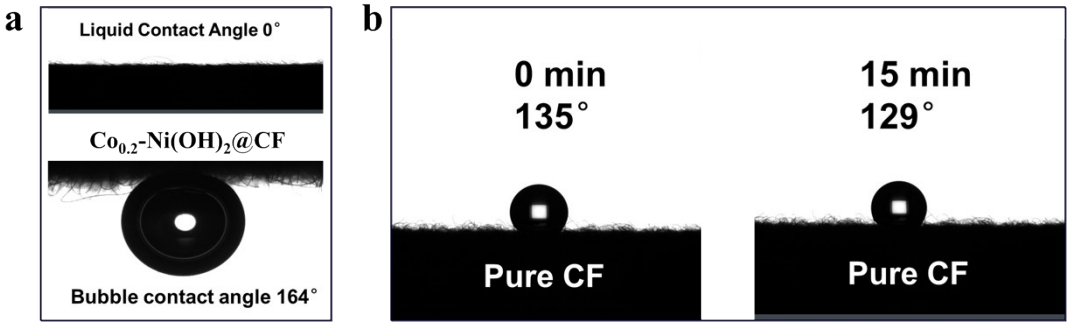

Fig. S8 (a)Wetting ability testing of $Co_{0.2}$-$Ni(OH)_2$@CF the contact angle (CA) is measured as 0° and Bubble contact angles (BCA) was measured as 164°. (b)Wetting ability testing of pure CF the contact angle is measured as 135°. After 15 min the contact angle is measured as 129°.

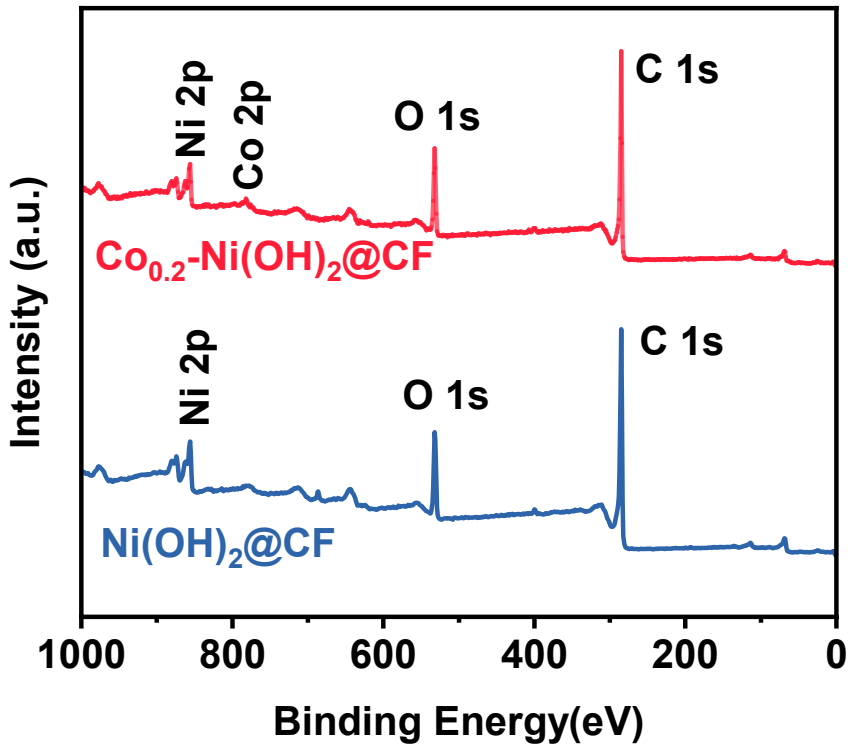

Fig. S9 XPS spectra of $Co_{0.2}$-$Ni(OH)_2$@CF and $Ni(OH)_2$@CF.

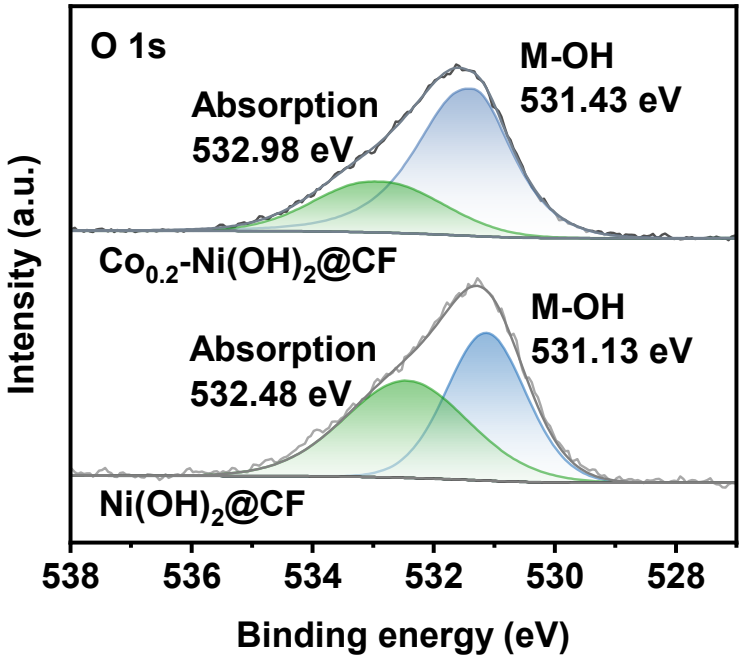

Fig. S10 O 1s XPS spectra of $Co_{0.2}$-$Ni(OH)_2$@CF and $Ni(OH)_2$@CF.

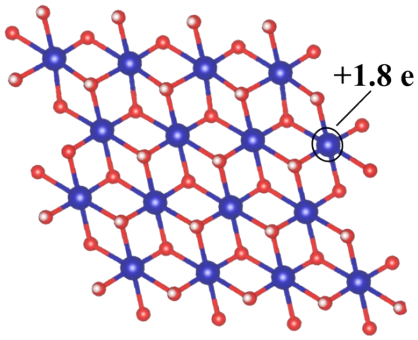

Fig. S11 Calculated Bader charges of $Co(OH)_2$.

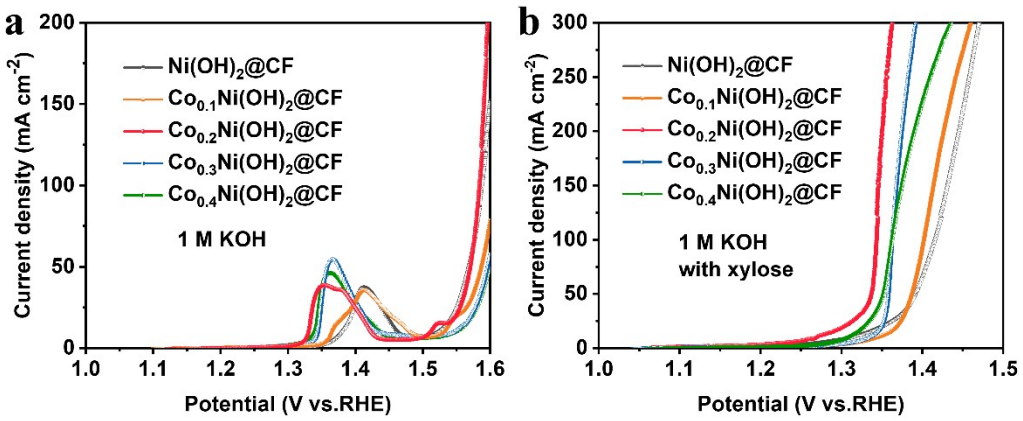

Fig. S12 (a) The corresponding LSV curves of post-activation samples including $Co_xNi(OH)_2$@CF at a scan rate of 2 mV s^{-1} in 1.0 M KOH. (b) The performance of $Co_xNi(OH)_2$@CF was measured in XOR.

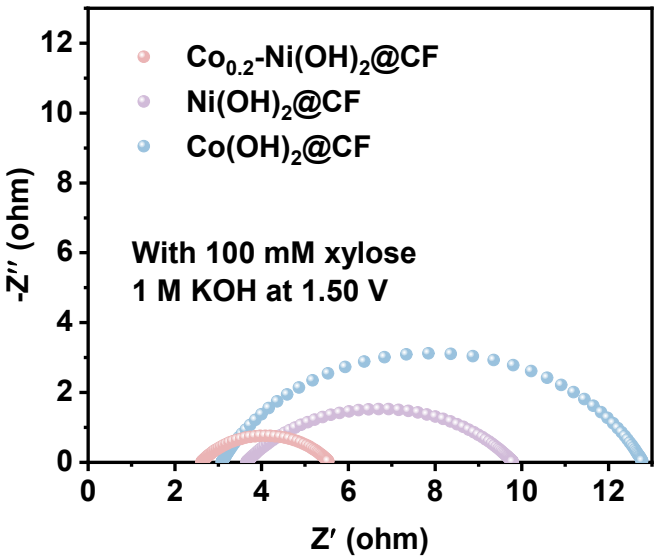

Fig. S13 The Nyquist plots at 1.5 V vs. RHE.

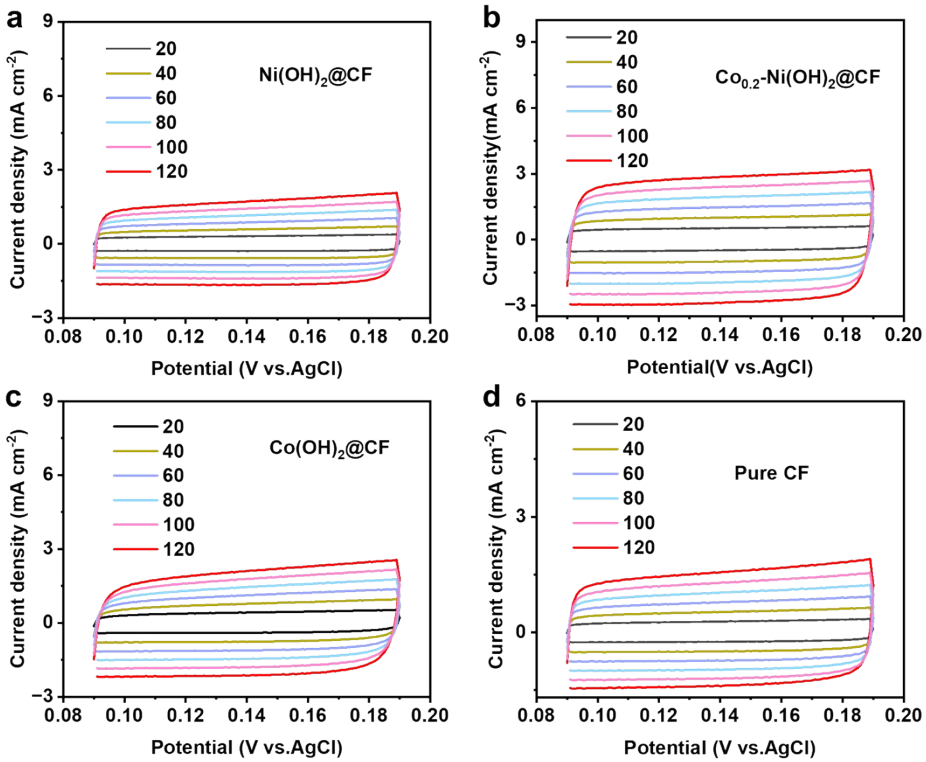

Fig. S14 Cyclic voltammetry curves of (a) $Co_{0.2}$-$Ni(OH)_2$@CF, (b) $Ni(OH)_2$@CF, (c) $Co(OH)_2$@CF, and (d) CF are taken in the potential region of 0.09-0.19 V vs. AgCl at scan rates from 20 mV s^{-1} to 120 mv s^{-1} in 1 M KOH solution.

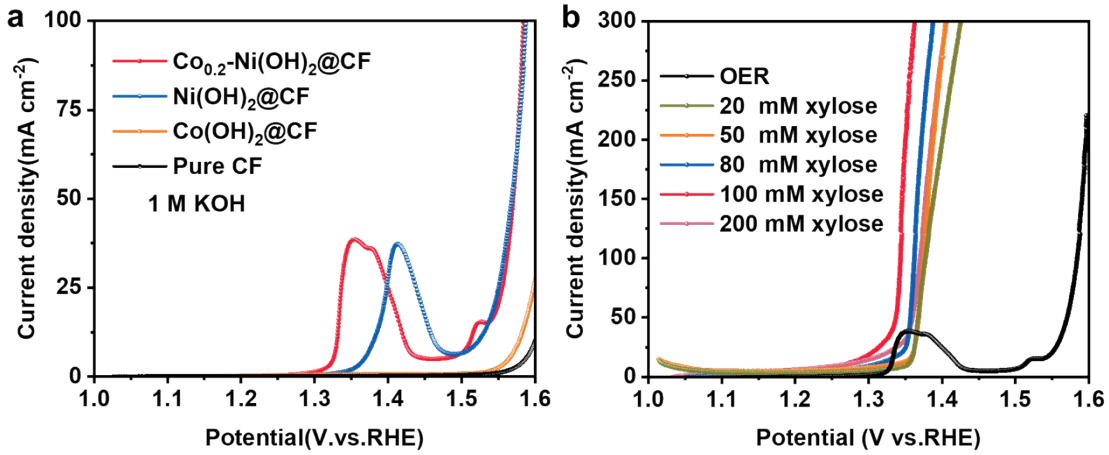

Fig. S15 (a) The corresponding LSV curves of post-activation samples including $Co_{0.2}$-$Ni(OH)_2$@CF, $Ni(OH)_2$@CF, and CF at a scan rate of 2 mV s^{-1} in 1.0 M KOH. (b) The performance of $Co_{0.2}$-$Ni(OH)_2$@CF was measured in terms of the OER and different xylose concentrations of XOR.

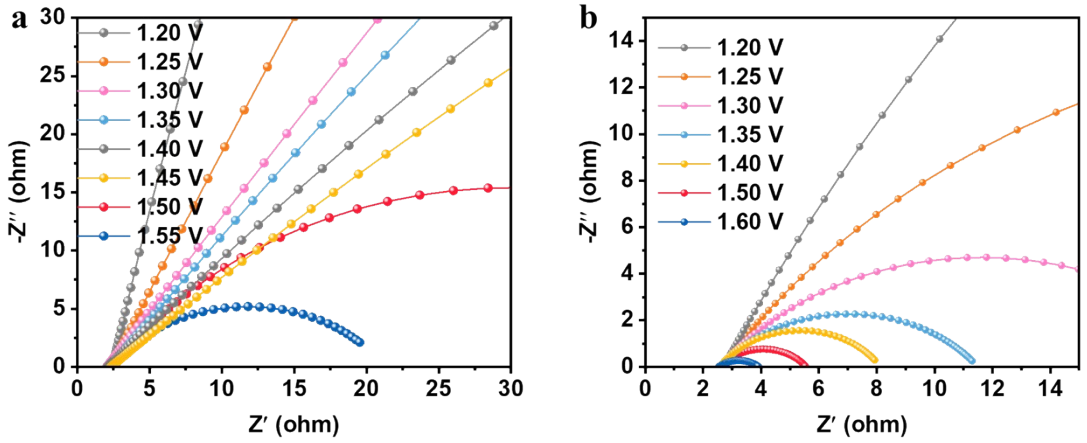

Fig. S16 Nyquist plots of $Co_{0.2}$-$Ni(OH)_2$@CF (a) in 1.0 M KOH and (b) 1.0 M KOH with 0.1 M xylose.

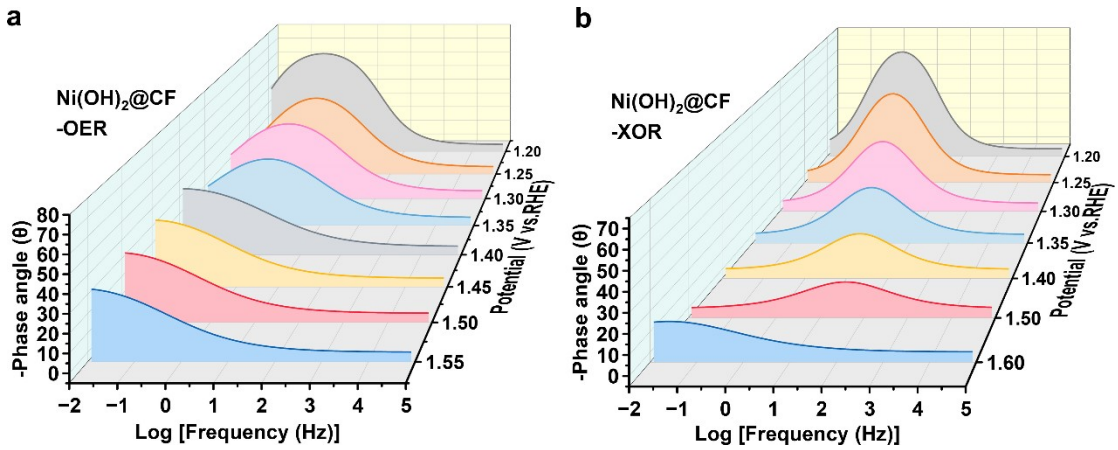

Fig. S17 Nyquist plots of $Ni(OH)_2$@CF (a) in 1.0 M KOH and (b) 1.0 M KOH with 0.1 M xylose.

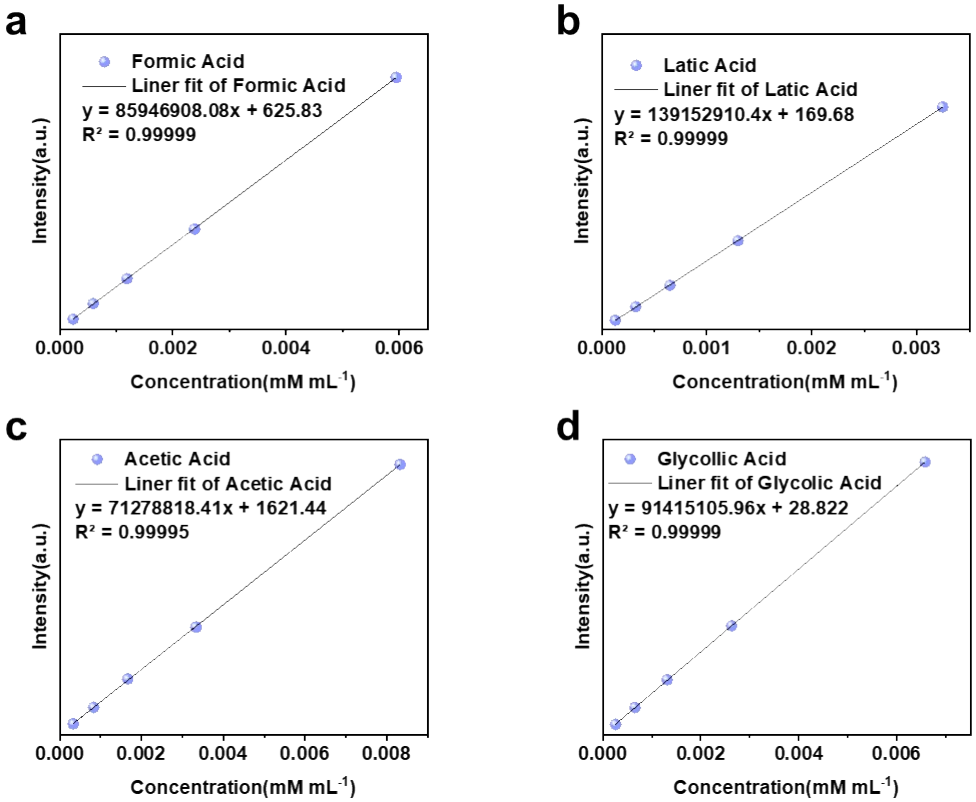

Fig. S18 Standard curves of (a-d) Formic Acid, Latic Acid, Acetic Acid, and Glycolic Acid.

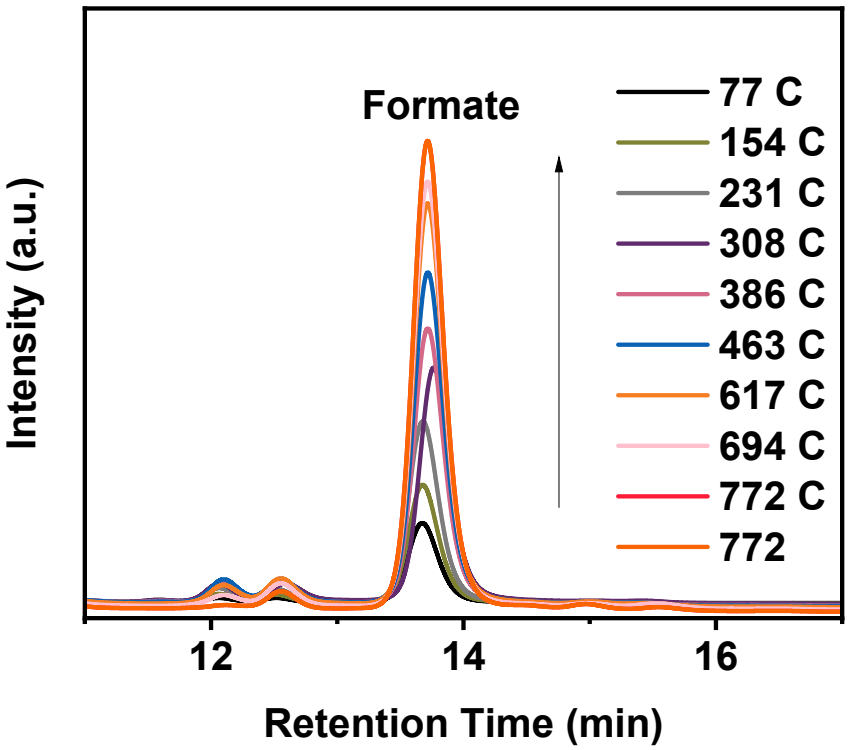

Fig. S19 The HPLC spectra in different charge at 1.65 V vs. RHE.

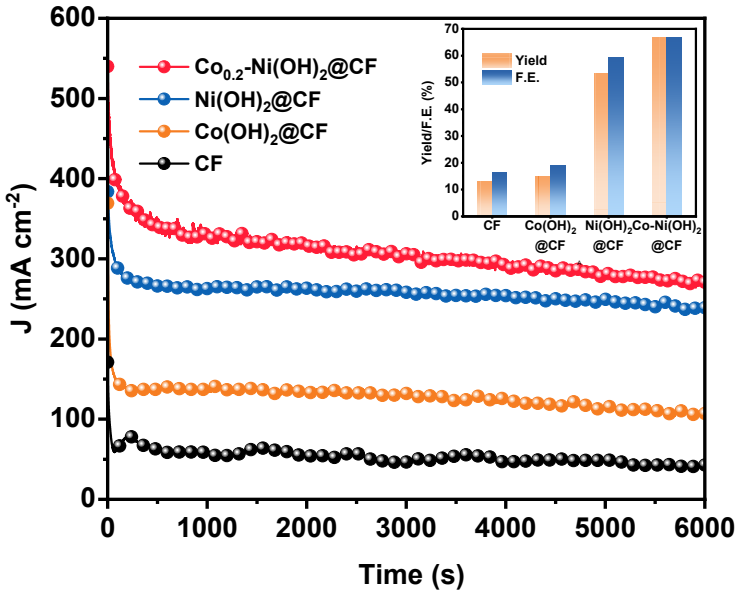

Fig. S20 I-t curves at 1.65 V vs. RHE of different samples (inset: formate yield and Faraday efficiency).

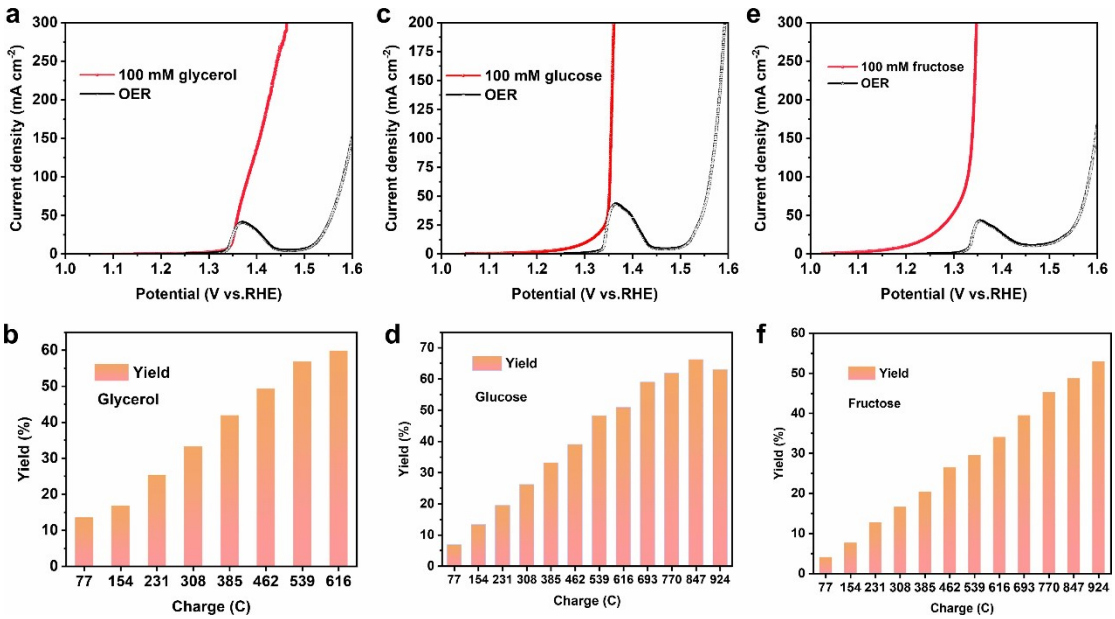

Fig. S21 The electrocatalysis performance of different organics substrate by $Co_{0.2}$-$Ni(OH)_2$@CF.

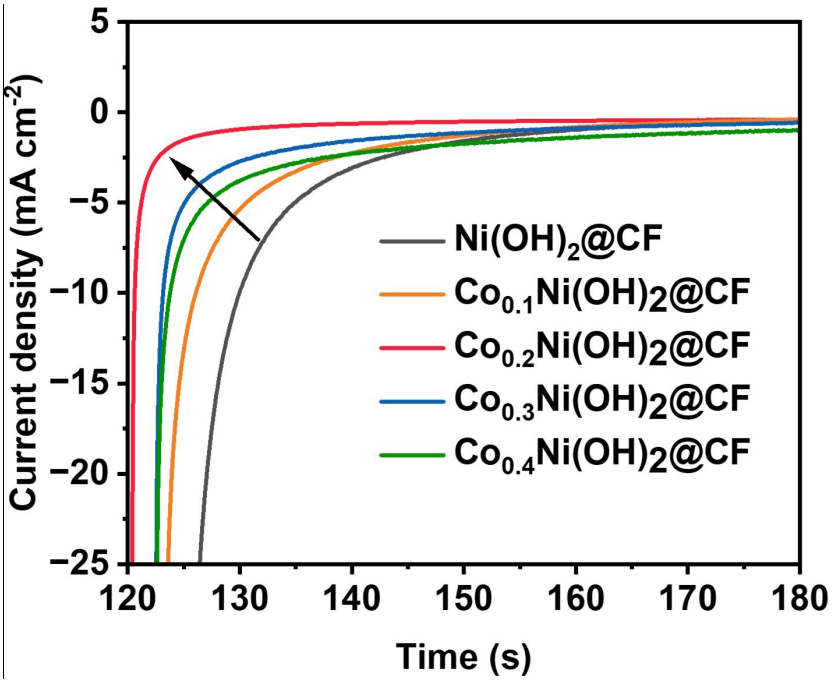

Fig. S22 Multi-potential chronoamperometry of different electrical catalyst.

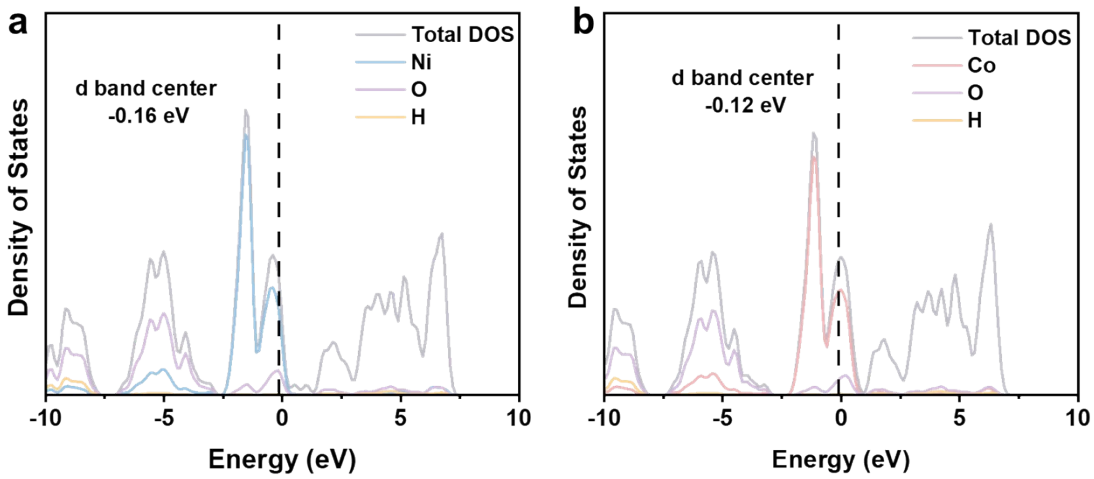

Fig. S23 The projected density of states of (a) $Ni(OH)_2$@CF and (b) $Co(OH)_2$@CF.

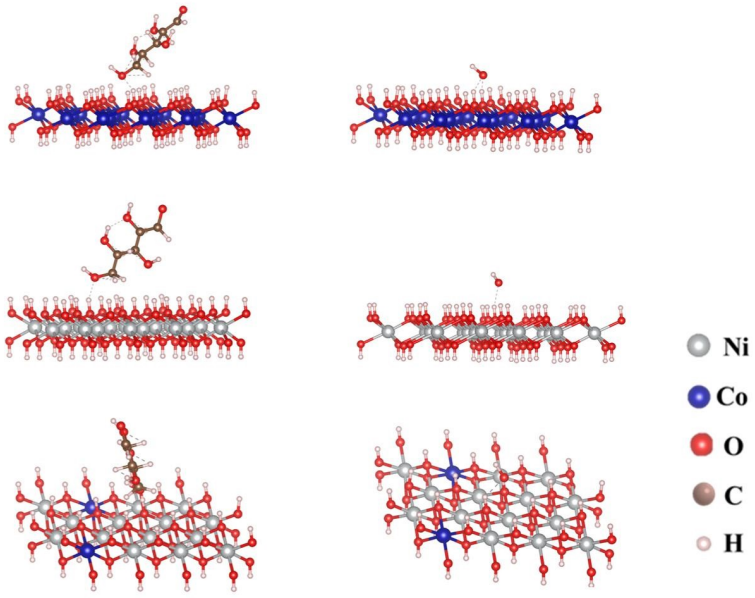

Fig. S24 The adsorption models toward xylose and OH^-.

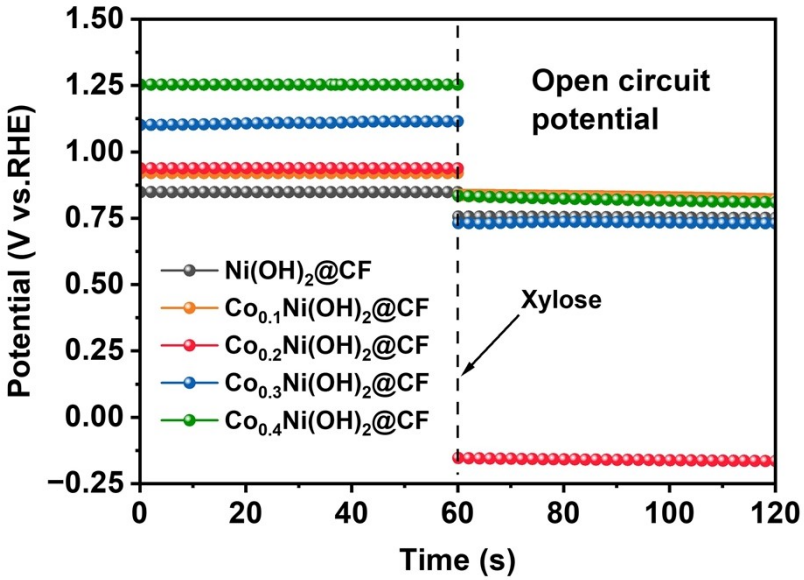

Fig. S25 Open circuit potential of different catalyst in KOH and 0.1 M xylose.

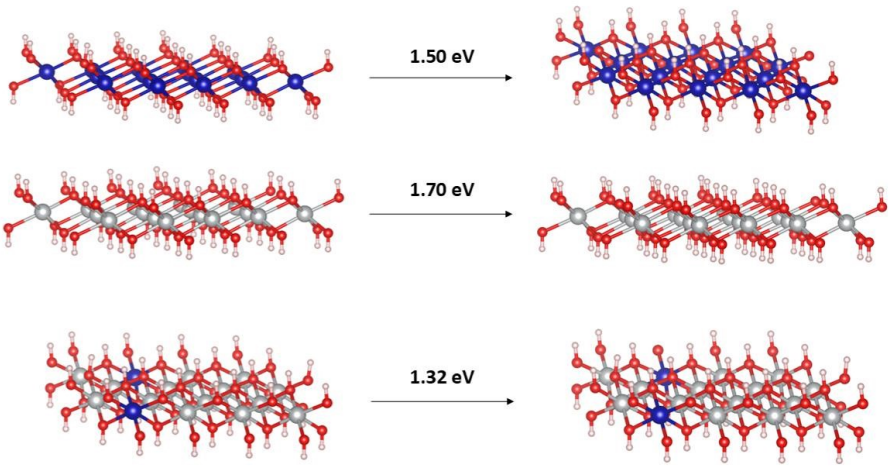

Fig. S26 Calculated free energy profile for deprotonation of the three models.

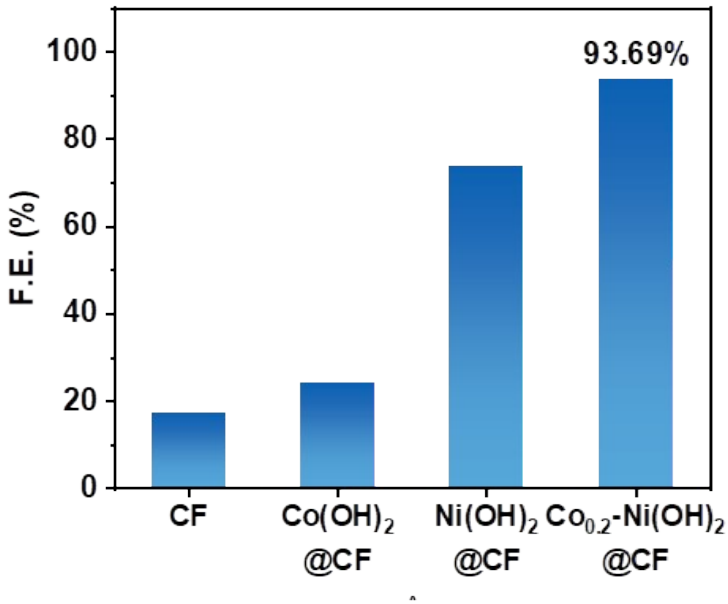

Fig. S27 The faraday efficiency of electrooxidation xylose to formate at current density of 250 mA cm^{-2}.

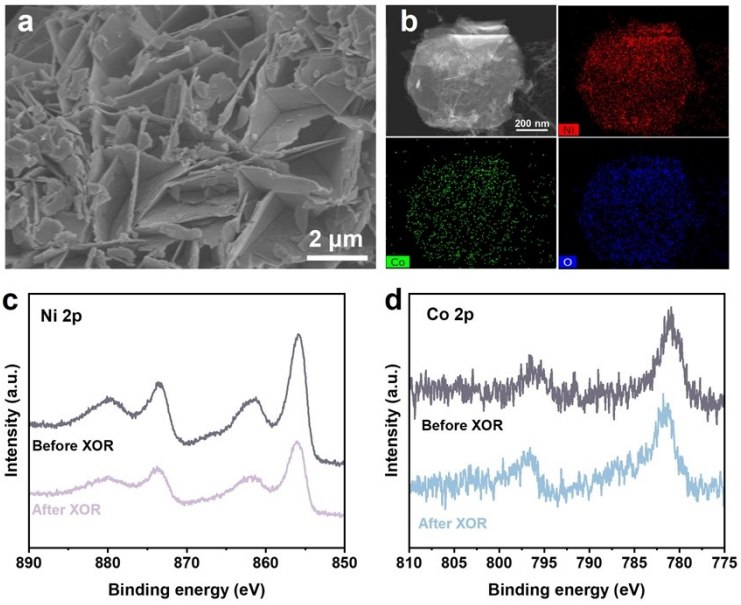

Fig. S28 Characterization of $Co_{0.2}$-$Ni(OH)_2$@CF after a 132-h stability test: (a) SEM pattern, (b) TEM pattern, (c) High-resolution Ni 2p spectrum, and (d) high-resolution Co 2p spectrum.

Tab. S1 Element contents of different sample measured by ICP OES.

Samples	Element content (%)	
	Co	Ni
$Co_{0.2}$-$Ni(OH)_2$	0.1115	0.9126

Tab. S2. Comparison of various organic molecule electrooxidation systems.

Electrocatalyst	Electrolyte	Voltage (V)	j (mA cm^{-2})	Ref.
$Co_{0.2}$-$Ni(OH)_2$@CF	1.0 M KOH + 0.1 M xylose	1.34	100	This work
$NiFeO_x$-NF	1.0 M KOH + 0.1 M glucose	1.32	100	[1]
NiCo hydroxide	1.0 M KOH + 0.1 M glycerol	1.35	100	[2]
Ni_3S_2-MoS_2/NF	1.0 M KOH + 0.01 M 5-hydroxymethylfurfural	1.35	50	[3]
O-NiMoP/NF	1.0 M KOH + 0.5 M urea	1.41	100	[4]
$Ni(OH)_2$/NF	1.0 M KOH + 0.5 M MeOH	1.36	100	[5]
$Ni_{0.1}Co_{0.9}$@NiSACoSA-NCNTs/CC	1.0 M KOH + 0.1 M glycerol	1.39	100	[6]
NiFeS	1.0 M KOH + 1 M glycerol	1.37	100	[7]
$Ni_{0.9}Co_{0.1}$-NC	1.0 M KOH + 0.33 M urea	1.35	100	[8]
NiCoO-NS/NF	1.0 M KOH + 0.1 M glucose	1.28	50	[9]
NiFeMnB	1.0 M KOH + 0.05 M 5-hydroxymethylfurfural	1.45	100	[10]
NiCo@Ni/CP	1.0 M KOH + 0.1 M xylose	1.29	100	[11]
CC@NiO/Ni_3S_2	1.0 M KOH + 0.2 M Ph-CH_2OH	1.42	85.7	[12]

References:

1. W.-J. Liu, Z. Xu, D. Zhao, X.-Q. Pan, H.-C. Li, X. Hu, Z.-Y. Fan, W.-K. Wang, G.-H. Zhao and S. Jin, *Nat. Commun.*, 2020, **11**, 265.
2. Z. He, J. Hwang, Z. Gong, M. Zhou, N. Zhang, X. Kang, J. W. Han and Y. Chen, *Nat. Commun.*, 2022, **13**, 3777.
3. S. Yang, Y. Guo, Y. Zhao, L. Zhang, H. Shen, J. Wang, J. Li, C. Wu, W. Wang, Y. Cao, S. Zhuo, Q. Zhang and H. Zhang, *Small*, 2022, **18**, 2201306.
4. H. Jiang, M. Sun, S. Wu, B. Huang, C.-S. Lee and W. Zhang, *Adv. Funct. Mater.*, 2021, **31**, 2104951.
5. J. Hao, J. Liu, D. Wu, M. Chen, Y. Liang, Q. Wang, L. Wang, X.-Z. Fu and J.-L. Luo, *Appl. Catal. B-Enivron.*, 2021, **281**, 119510.
6. Q. Zhang, X. Zhang, B. Liu, P. Jing, X. Xu, H. Hao, R. Gao and J. Zhang, *Angew. Chem. Int. Ed.*, 2025, **64**, e202420942.
7. H. Ren, J. Zhang, T. Hu, Y. Li, H. Zhao, E. Luo, H. Xiao, M. Zhao, J. Tang and J. Jia, *Green Chemistry*, 2025, **27**, 10711-10722.
8. Z. Ma, X. Liu, H. Wang, L. Xie, Z. Sun, H. Zhan, X. Mi, S. Zhan and Q. Zhou, *Adv. Energy Mater.*, 2025, e02563.
9. Z. Ma, H. Guo, P. Wang, L. Dai, S. Zhan and F. Shen, *Chem. Eng. J.*, 2025, **514**.
10. B. Liu, L. Shi, W. Cai, F. Zhang, S. Li, X. Liu, Y. Liu, P. Ren, B. Li and S. Liu, *Angew. Chem. Int. Ed.*, 2025,.202424345.
11. J. Gan, N. Wang, Y. Yang, O. Itana, E. Kifle, K. Yilma, W. Yang, Z. Chen, Y. Song, R. Xia, S. Admassie, E. Iwuoha, L. Zhong, Y. Liu and X. Peng, *Appl. Catal. B: Environ. Energy* 2025, **363**, 124792.
12. R. Li, P. Kuang, L. Wang, H. Tang and J. Yu, *Chem. Eng. J.*, 2022, **431**, 134137.